buildings

MDPI

Article

An Innovative Composite Wall Inner Tie System Applied to Reinforced Concrete Modular Integrated Construction

Xiaokang Zou [1], Jiang Huang [2], Wenjie Lu [1,*], Jun Shi [2], Sunny Au [2], Zhen Zhao [2], Tian Shi [2], Daniel Kan [1] and Yang Zhang [1]

[1] Structures Research Hub, China State Construction Engineering (Hong Kong) Ltd., Hong Kong, China; connie_zou@cohl.com (X.Z.); daniel_kan@cohl.com (D.K.); yang.zhang@cohl.com (Y.Z.)
[2] China State Construction Engineering (Hong Kong) Ltd., Hong Kong, China; huangjiang@cohl.com (J.H.); shijun@cohl.com (J.S.); sunny_au@cohl.com (S.A.); zhen_zhao@cohl.com (Z.Z.); shitian@cohl.com (T.S.)
* Correspondence: wenjie.lu@cohl.com

Abstract: The application of reinforced concrete modular integrated construction (MiC) has gained popularity in Hong Kong, but challenges still exist in the temporary tying of side walls during composite wall construction. This paper presents an innovative inner tie system for composite walls, applied in a MiC project in Hong Kong. The system's components are installed on the side walls of precast modules in the factory without the need to penetrate through the walls. After transport to the site, by rotating the loop on-site to engage the hook, the tying effect is achieved during on-site concrete pouring between the interstitial space of two modules. This system eliminates the use of tie bolts that penetrate precast side walls, allowing for comprehensive interior fitting-out in the factory and minimizing disruptions to internal decoration during on-site construction. The paper presents the system's mechanism, nonlinear Finite Element Analysis (FEA) simulation, section size optimization, and validation through tensile and punching shear tests. Furthermore, an instrumented mockup module assembly was carried out, and the system was eventually applied in a real MiC project. The system can effectively control the horizontal deformation of MiC module side walls within a limit. Compared to current existing tying methods, this system offers easy installation, load-bearing reliability, adaptability to certain construction errors, savings on manpower and construction time, and also a decrease in construction waste and carbon emission. It will provide a valuable reference for future MiC projects.

Keywords: modular integrated construction (MiC); composite wall; wall tie; deformation; optimization; nonlinear finite element analysis

check for updates

Citation: Zou, X.; Huang, J.; Lu, W.; Shi, J.; Au, S.; Zhao, Z.; Shi, T.; Kan, D.; Zhang, Y. An Innovative Composite Wall Inner Tie System Applied to Reinforced Concrete Modular Integrated Construction. *Buildings* **2024**, *14*, 3052. https://doi.org/10.3390/buildings14103052

Academic Editor: Patrick Tang

Received: 7 August 2024
Revised: 11 September 2024
Accepted: 19 September 2024
Published: 25 September 2024

Copyright: © 2024 by the authors. Licensee MDPI, Basel, Switzerland. This article is an open access article distributed under the terms and conditions of the Creative Commons Attribution (CC BY) license (https://creativecommons.org/licenses/by/4.0/).

1. Introduction

In recent years, Hong Kong has encountered challenges such as local labor shortages, expensive construction costs, and significant demands for the advancement of the construction industry. Since 2017, modular integrated construction (MiC) has been widely applied in Hong Kong to mitigate pressure on the local construction sector. The MiC approach involves transferring numerous construction processes to the factory for completion, thereby leading to a substantial reduction in construction duration and complexity.

After two adjacent reinforced concrete MiC modules are installed on-site, the narrow space between them is filled with concrete to form a composite wall. To prevent undue deformation to the thin side walls during concrete casting, horizontal pressure is typically counterbalanced by tie rods penetrating the side walls. However, this approach impacts the interior decoration of the modules and necessitates extensive on-site decoration and repairment works.

A composite wall construction method is commonly used by utilizing precast side walls solely as formworks for pouring concrete between two modules and extending

stirrups to the gap from the precast side walls. The stirrups, staggered vertically and partially overlapping horizontally, facilitate the pouring of concrete into the middle gap of the composite wall [1,2]. In this approach, the stirrups are unable to serve as temporary support during on-site concrete casting. Consequently, the precast wall requires greater thickness to withstand the lateral pressure from the wet concrete, resulting in an increase in the weight of the precast MiC module, elevated transportation and lifting complexity, and a decrease in the usable area of the building. In Singapore, an alternative composite wall construction method was employed by flexible steel wires instead of stirrups. Flexible wires embedded in two adjacent precast side walls partially overlapped on the plane, and vertical steel bars were inserted through the overlapping sections, followed by grouting the gap between the two precast walls [3]. Additionally, the University of Hong Kong has devised a new horizontal connection for multi-story and high-rise concrete MiC buildings [4], eschewing stirrups or wires extending from precast side walls, and necessitating merely a 20 mm gap for grouting. Both of these approaches require thicker precast side walls to withstand grouting pressure.

To reduce side wall thickness and minimize impact on the factory module internal decoration rates, a composite wall with a steel truss tying system was developed [5,6], eliminating the need for holes on one side wall. However, holes still need to be reserved on the other side wall to install tie rods before pouring concrete into the module gap. Further refinement involved embedding steel angles with slots into the precast side walls and inserting wedge connectors into the slots to link the side walls [7]. The construction convenience and contact surface slippage of this refinement require additional verification.

The utilization of new building materials also has the potential to address the current challenges in the MiC construction industry [8–10]. Specifically, employing lightweight, high-performance, and recyclable materials can significantly enhance construction efficiency. These innovations not only offer structural advantages but also represent a valuable opportunity to further advance modern industrialized construction (MiC) and foster ecological sustainability. In seeking to preserve interior decoration and withstand lateral pressure on the thin side walls of precast modules during concrete pouring, a new inner tie system for MiC composite wall construction was invented [11]. This system improves the traditional method of penetrating tie rods through the precast side walls before pouring concrete into the module gap and facilitates the completion of the MiC module's interior decoration in the factory while ensuring that the on-site module connection does not compromise the interior decoration. This system also improves the other commonly used method of using thicker side walls to take on-site concrete pouring pressure, which makes the MiC module lighter, usable area larger, and site lifting easier. In other words, each MiC module may be designed with larger dimensions for a more comfortable living experience when the maximum lifting capacity on-site is determined.

Novel systematic optimization techniques have been developed for elastic and inelastic structures under static and dynamic loads, with extensive optimization studies conducted [12–18]. This paper first presents the system's mechanism using a nonlinear Finite Element Analysis (FEA) simulation. Based on developed optimization techniques and experiences, member size optimization is made. Then its validation through tensile and punching shear tests are given. In addition, an instrumented mockup module assembly is carried out to verify that the system could effectively control the horizontal deformation of MiC module side walls, and the system is eventually applied in a real MiC project.

2. Mechanism of the System

The innovative internal tie system comprises H-shaped steel embeds, hooks, and loops (as depicted in Figure 1), which work together with MiC side walls to resist the horizontal pressure of wet concrete and restrain the side walls' lateral deformation during concrete pouring into the cavity encompassed by two MiC modules. The hooks and loops feature serrated contact surfaces and are affixed to the embeds through welding. The internal tie

spacing can be determined based on the lateral pressure magnitude, loaded area of each tie, and its own tensile capacity.

The 3D Building Information Modeling (BIM) view for two MiC modules is shown in Figure 2. The composite wall construction procedure is outlined as follows:

(1) The modules are prefabricated in the factory, and embeds are installed in the side walls.
(2) The hooks are welded to the steel plates in the end of the embeds, and the loop holders with loops are welded to the end steel plates of the embeds.
(3) The N-th module is installed on-site.
(4) Rebars are fixed between the two modules. The loops of the (N + 1)-th module are pulled upward with ropes and the ropes are fixed onto the top of the (N + 1)-th module.
(5) The (N + 1)-th module is installed on-site.
(6) The worker cuts the ropes from the top of the module to release loops, and the loops fall to the left under their self-weight, as shown in Figure 3a.
(7) Concrete is poured into the gap between the N-th and (N + 1)-th modules, as shown in Figure 3b.

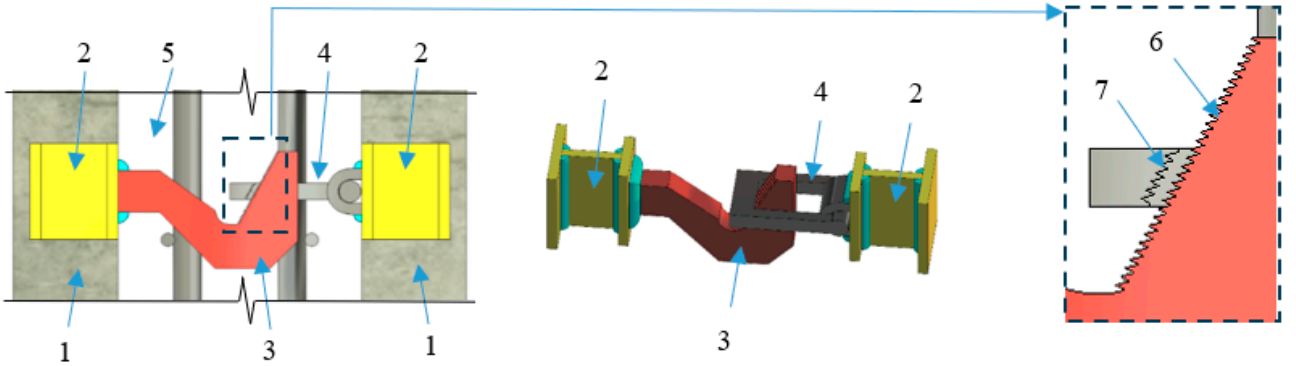

1—precast side wall, 2—embed, 3—hook, 4—loop, 5—cast-in-situ concrete, 6—serrated surface on hook, 7—serrated surface on loop

Figure 1. Diagram of the inner tie system.

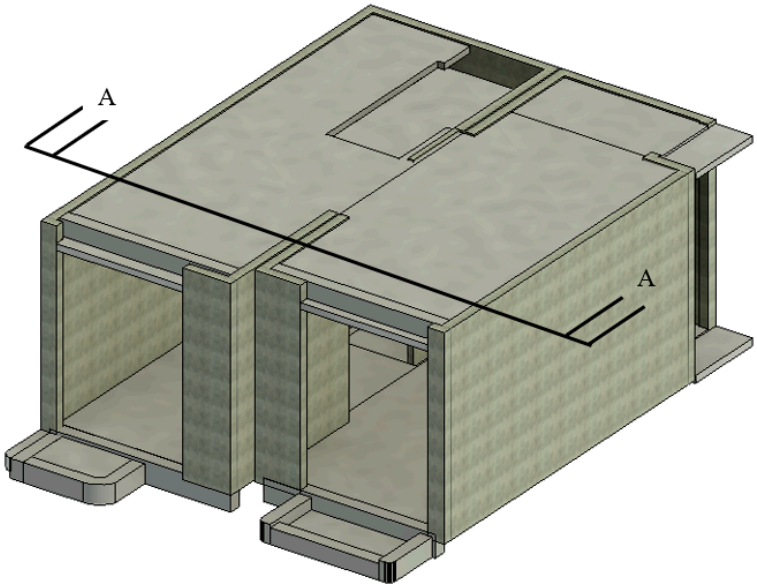

Figure 2. The 3D BIM view for two adjacent MiC modules.

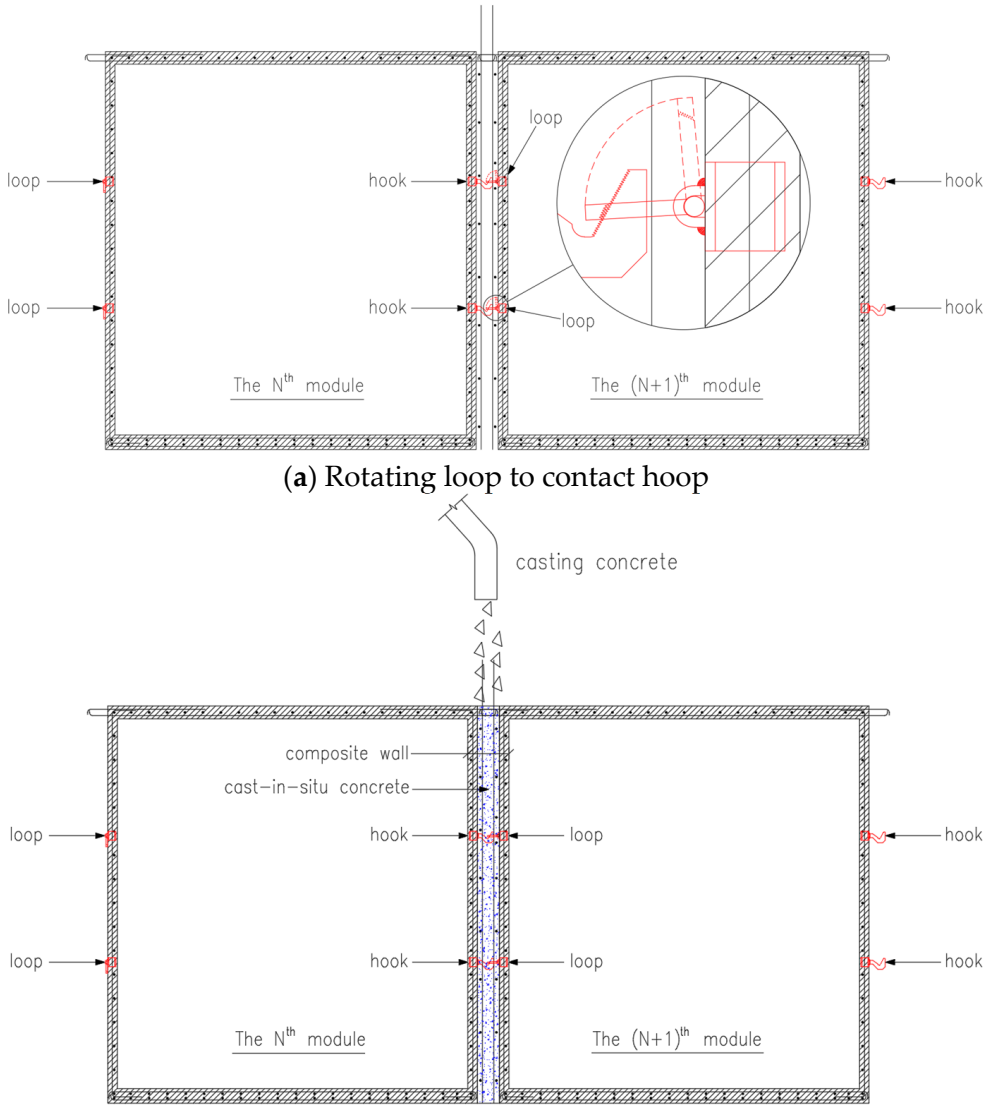

Figure 3. Section A-A for the key construction status of the system.

3. Numerical Simulation for the Inner Tie System

3.1. Design Parameters

The inner tie system is composed of S355J0 grade steel, and its design parameters are detailed in Table 1. In the elastoplastic analysis using FEA software Ansys V16, the ideal elastoplastic assumption is employed, neglecting the strain hardening of steel.

Table 1. Design parameters for the steel grade with S355J0.

Steel Grade	Steel Thickness (mm)	Design Strength p_y (N/mm^2)	Elastic Modulus (N/mm^2)	Poisson's Ratio
S355J0	≤16	355	2.05×10^5	0.3
	>16, ≤40	345		

3.2. Tension Force and Initial Tie Member Sizes

According to the design concrete pressure envelope (Figure 4) and the following Equation (1) in CIRIA Report 108 [19], the concrete fluid pressure acting on the side wall

of the module experiences a linear increase to P_{max} at a depth of P_{max}/D, and keeps this value to the bottom level.

$$P_{max} = D\left[C_1\sqrt{R} + C_2K\sqrt{H - C_1\sqrt{R}}\right] \text{ or } DhKN/m^2, \text{whichever is the smaller} \quad (1)$$

where,

C_1—is the coefficient dependent on the size and shape of formwork;
C_2—coefficient dependent on the constituent materials of the concrete;
D—weight density of concrete;
H—vertical form height;
h—vertical pour height;
T—concrete temperature at placing;
K—temperature coefficient taken as $\left(\frac{36}{T+16}\right)^2$;
R—the rate at which the concrete rises vertically up the form.

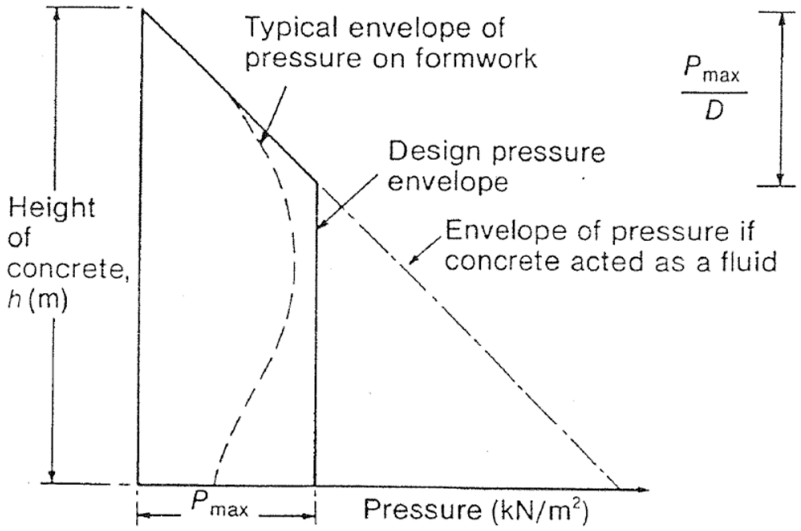

Figure 4. Concrete pressure envelope in CIRIA report 108 [19].

For a project example in Equation (1), if some variable values are known as shown in Table 2, the lateral concrete pressure P_{max} can be determined and its distribution is shown in Figure 5.

$$\begin{aligned} P_{max} &= D\left[C_1\sqrt{R} + C_2K\sqrt{H - C_1\sqrt{R}}\right] \\ &= 24.0\cdot\left[1.0\sqrt{1.0} + 0.3\cdot 0.612\sqrt{2.925 - 1.0\sqrt{1.0}}\right] \\ &= 30.11 \text{ kPa} \end{aligned}$$

$$Dh = 24.0 \times 2.925 = 70.2 \text{ kPa} > 30.11 \text{ kPa}$$

$$P_{max} = 30.11 \text{ kPa}$$

$$P_{max}/D = 1.25 \text{ m}$$

Table 2. Variable values for an example.

Variable	C_1	C_2	D	H	h	T	K	R
Value	1.0	0.3	24.0 kN/m^3	2.925 m	2.925 m	30 °C	0.612	1.0 m/h

By assuming inner ties are distributed with no more than 1.0 m spacing vertically and horizontally, the tension force T taken by one inner tie can be estimated for wall tie design according to Equation (2) below.

$$T = P_{max} \times \text{Loading Area} = 30.11 \times 1.0 \times 1.0 = 30.11 \text{ kN} \quad (2)$$

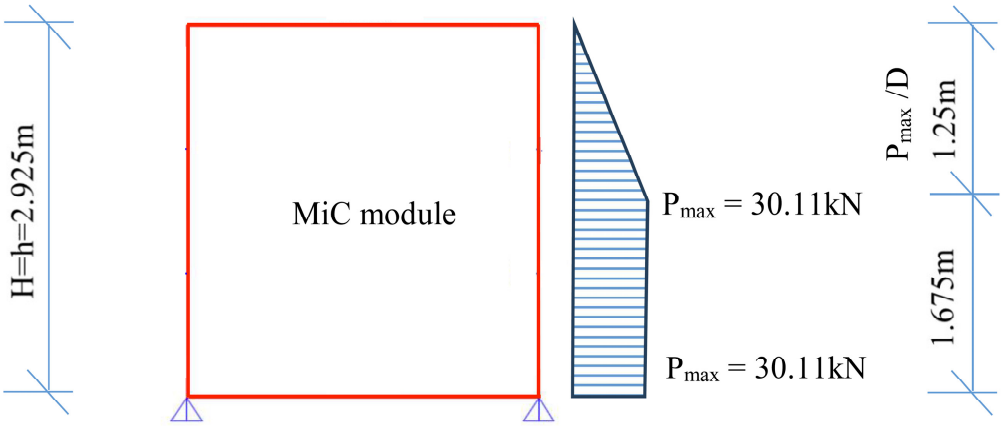

Figure 5. Concrete pressure envelope for the example.

To estimate the preliminary dimension of the inner tie, one simplified method is used to check several key sections under the combined effect of axial force, bending, and shear based on local design codes. The unfactored tension force T is assumed to act on the top of the hook as the worst scenario and the dimension of four main sections (such as Cross-section 1–Cross-section 4 in Figure 6a) are adjusted and checked to meet the local design code requirements. For the loop's dimension, T is applied to the left end as shown in Figure 6b. The original scheme determined by the simplified method is shown in Figure 6a,b.

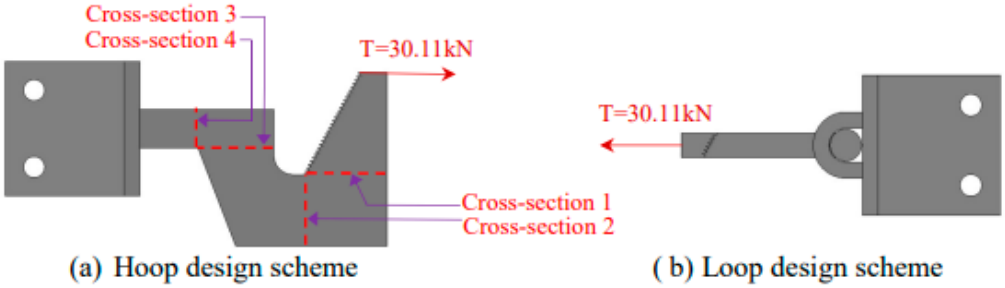

Figure 6. Preliminary scheme determined by the simplified method.

3.3. Serrated Surface Design

To prevent slippage between the hook and loop, serrated contact surface (Figure 1c) is designed to ensure reliable tension force transmission. If perfectly engaged, all seven teeth can share the tension force. But for a safety perspective, only three teeth are considered to take all the tension force. The forces are equally applied to the tips of three teeth, and the moment and shear capacity at the root of the teeth are checked according to local design code.

3.4. Construction Tolerances

Construction errors may occur during the installation of embeds and welding of hooks/loops in the factory, as well as during the on-site placement of prefabricated modules. Based on practical experiences, ±3 mm tolerance is allowed for fabrication in the factory and ±5 mm tolerance is reserved for on-site installation. Hence, the total construction

tolerance of ±8 mm in X direction is taken into consideration in the design of the tie system, as delineated in Figure 7.

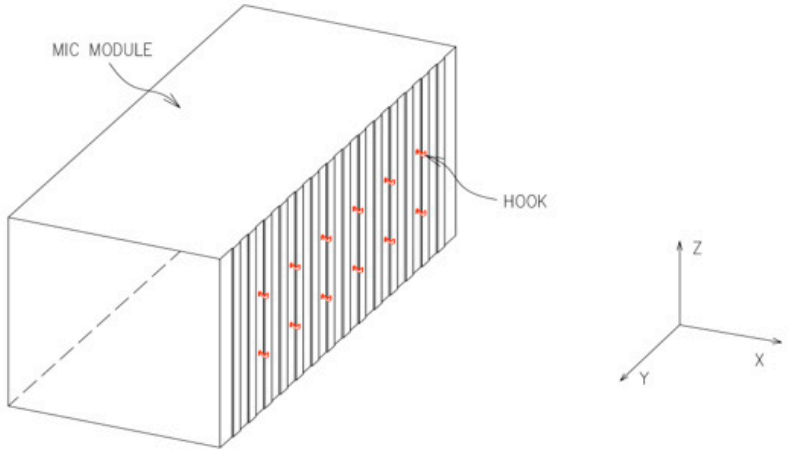

(**a**) Index of X and Y directions for one MiC module

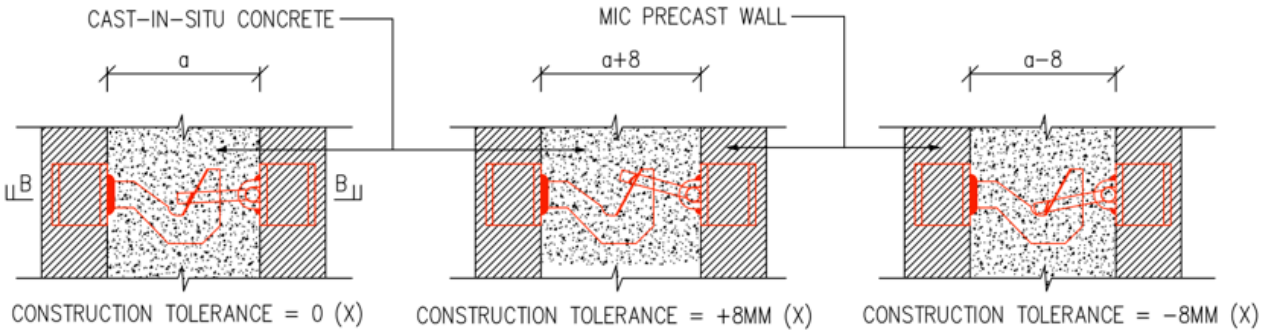

(b) Allowed tolerances in X direction

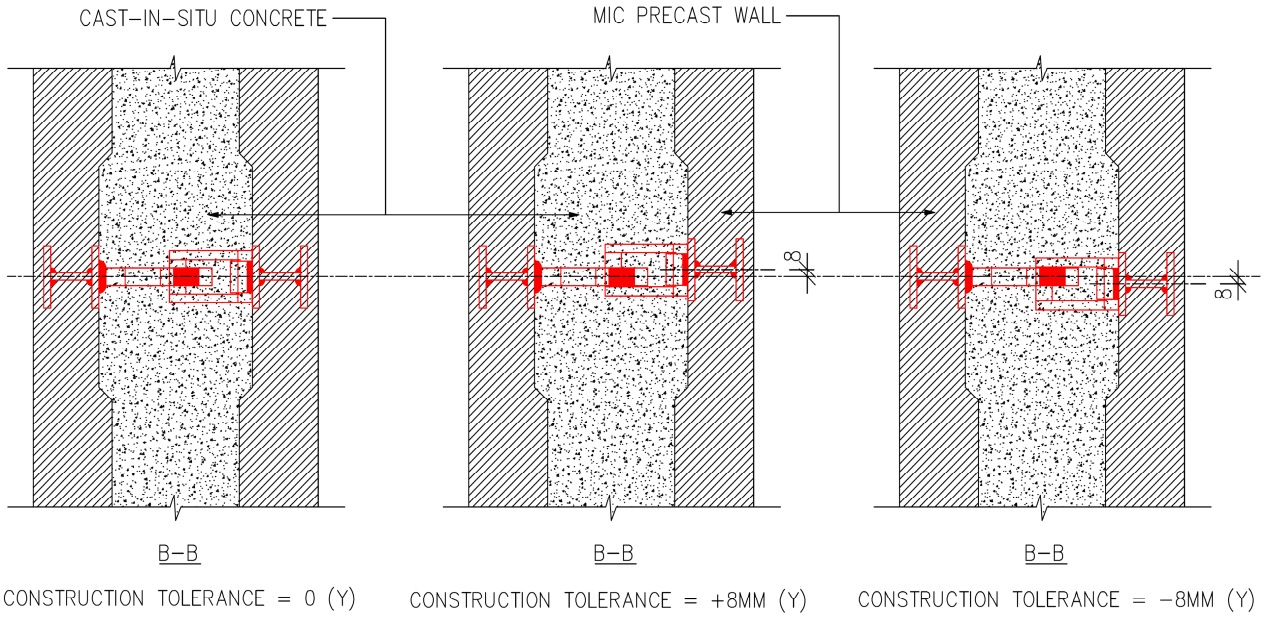

(**c**) Allowed tolerances in Y direction

Figure 7. Allowable maximum construction tolerances for the inner tie system.

As construction tolerances in X and Y directions may dominantly impact the tensile capacity and stiffness of the inner tie system compared with Z direction, six cases are

considered to simulate different construction tolerance scenarios in the inner tie analysis and design, as shown in Figure 7. The six cases are defined below:

Case 1: +8 mm construction tolerance in X direction, no tolerance in Y direction;
Case 2: no construction tolerance in X and Y directions;
Case 3: −8 mm construction tolerance in X direction, no tolerance in Y direction.
Case 4: +8 mm construction tolerance in X direction, +8 mm tolerance in Y direction;
Case 5: no construction tolerance in X direction, +8 mm tolerance in Y direction;
Case 6: −8 mm construction tolerance in X direction, +8 mm tolerance in Y direction.

3.5. Optimized Scheme and Section Sizes

As mentioned in Section 3.2 and shown in Figure 8a, the approximate section sizes of the inner tie system were initially determined through the simplified method (Figure 6). Subsequently, they were optimized by using nonlinear FEA software Ansys and construction tolerances were incorporated into the analysis and design. The specially shaped section of the hook was modeled through solid elements. Horizontal tensile force of 30.11 kN was applied to the inner tie system. After analysis, parts of the hook with small stresses were eliminated, while parts with significant stresses were strengthened. Finally, the optimized scheme is shown in Figure 8b. The stress distributions of the initial scheme and optimized scheme under Case 2 are illustrated in Figure 9.

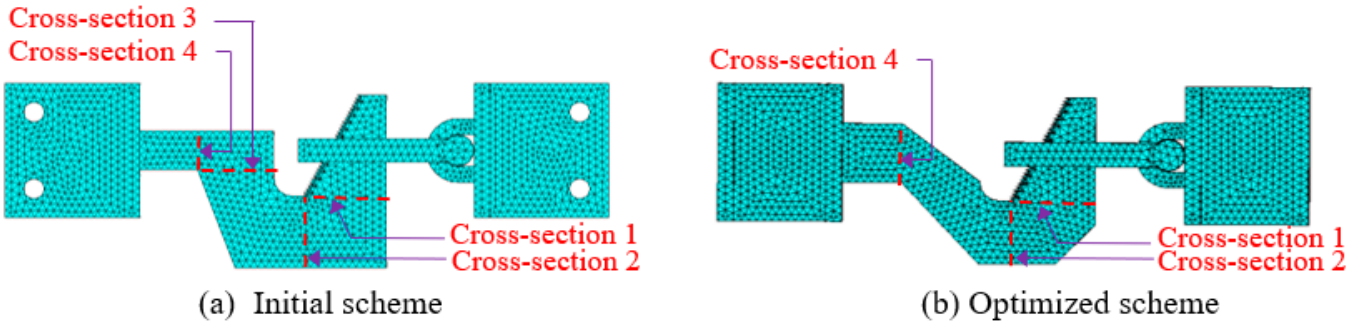

Figure 8. FEA solid elements for the initial and optimized schemes.

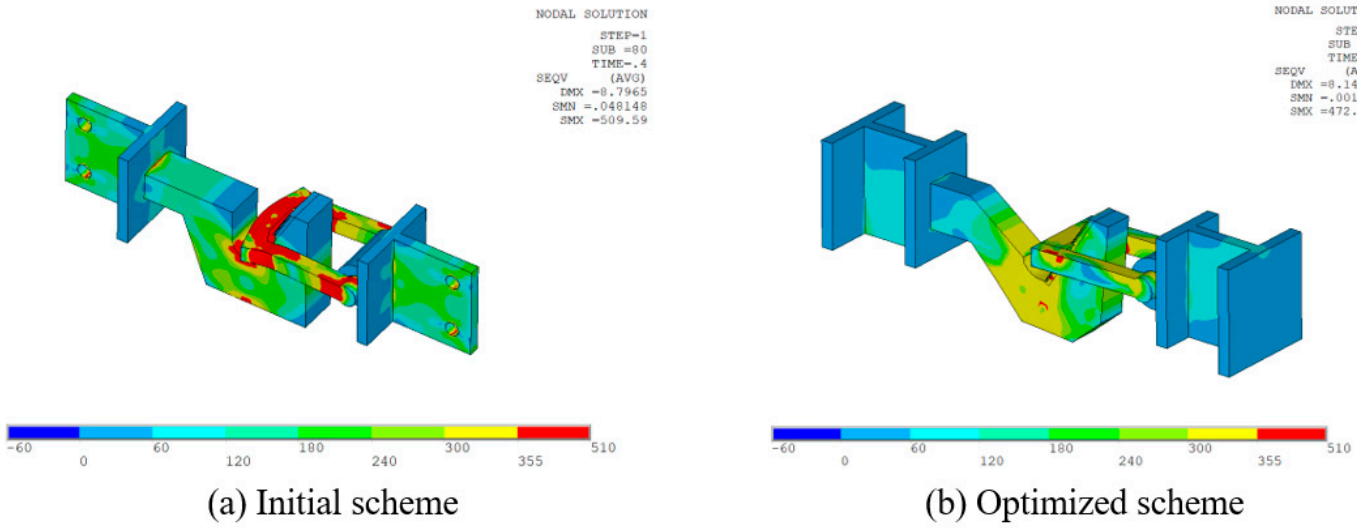

Figure 9. Stress diagram for the initial scheme and the optimized scheme under Case 2.

Key cross-section sizes before and after optimization are summarized in Table 3. The weight of hook was reduced from the initial 1.56 kg to the final 0.88 kg (43.6% reduction) after optimization.

Table 3. Section size and weight.

Item	Initial Scheme		Optimized Scheme	
	Section Width (mm)	Section Thickness (mm)	Section Width (mm)	Section Thickness (mm)
Cross-section 1	44	30	44	20
Cross-section 2	37	30	32	20
Cross-section 3	40	30	Not Applicable	Not Applicable
Cross-section 4	20	30	30	20
Weight	1.56 kg		0.88 kg (43.6% reduction)	

Note: The locations of Cross-sections 1~4 are shown in Figure 8.

In this project, the precast side walls are not considered as parts of the shear wall and only the cast-in-situ shear wall between precast side walls are used to withstand wind load and upper floors' gravity load. With consideration of the interior decoration protection, it may be reasonable to set the allowable horizontal deformation of each precast side wall to 4 mm during concrete casting in the middle gap of two modules. Consequently, the total deformation of 8 mm (4 mm × 2) becomes a key parameter for analysis and design.

For the optimized scheme, the FEA results of tensile force at 8 mm deformation under the six tolerance cases are summarized in Table 4. Cases 4~6 demonstrated only very little tensile capacity variations (around −3.5~11.3%) compared to Cases 1~3, respectively, which indicates that the construction tolerance in Y direction does not have a significant impact to the system's capacity and stiffness.

Table 4. Analyzed tensile force at 8 mm deformation under six tolerance cases.

Case	Tension at 8 mm Deformation (kN)
Case 1	34.20
Case 2	63.97
Case 3	68.97
Case 4	38.08
Case 5	64.38
Case 6	66.58

4. Experimental Verification

Through the analysis in the preceding section, the member sizes of the inner tie system were established. To verify the analysis results, a series of mechanical tests including tensile and punching shear tests were carried out in a mechanics lab and their results are introduced as follows.

4.1. Tensile Test

Five identical samples (referred to as "S1"–"S5") were produced for destructive tensile tests. The material strength indicated on the mill certificate of S355J0 steel plates is detailed in Table 5. The five samples were used to simulate three different construction tolerance scenarios below:

S1, S2, and S5: construction tolerance of +8 mm only in X direction;
S3: no construction tolerance;
S4: construction tolerance of −8 mm only in X direction.

When test load became bigger, shear failure occurred at the root of the loop in S1 (Figure 10) with the increase in test load. Similar failure modes were observed for all other tests (Figure 11). Although some deformation was observed on the serrated contact surfaces of the hooks and loops, failure was not reached.

Table 5. Material strength shown on the mill certificate of S355J0 steel plates.

Steel Grade	Steel Thickness (mm)	Yield Strength p_y (N/mm^2)	Ultimate Strength f_u (N/mm^2)
S355J0	16	418~459	549~566
	20	384~429	521~536



(a) Before loading (b) After loading

Figure 10. Tensile testing for Sample S1.



Figure 11. Failed Samples S1~S5.

The load vs. deformation curves under tensile testing for Sample S1~S5 are illustrated in Figure 12a–e. The test tensions (T_{Test}) are summarized in Table 6 when the sample's deformation reached 8 mm. The ultimate tensile force and the corresponding ultimate deformation of the five samples are summarized in Table 7. The ultimate deformations for all test samples are much larger than 8 mm, indicating the inner ties have sufficient deformability before failure. The ultimate tension and deformation for Sample S1, S2, and S5 have 13% and 21% differences, respectively, which may be caused by the welding during manufacturing process and/or slight positioning differences before testing.

Table 6. Tension at 8 mm deformation of sample tests.

Case	Test Sample	Tension at 8 mm Deformation T_{Test} (kN)
Case 1	S1	33
	S2	33
	S5	31
Case 2	S3	43
Case 3	S4	51

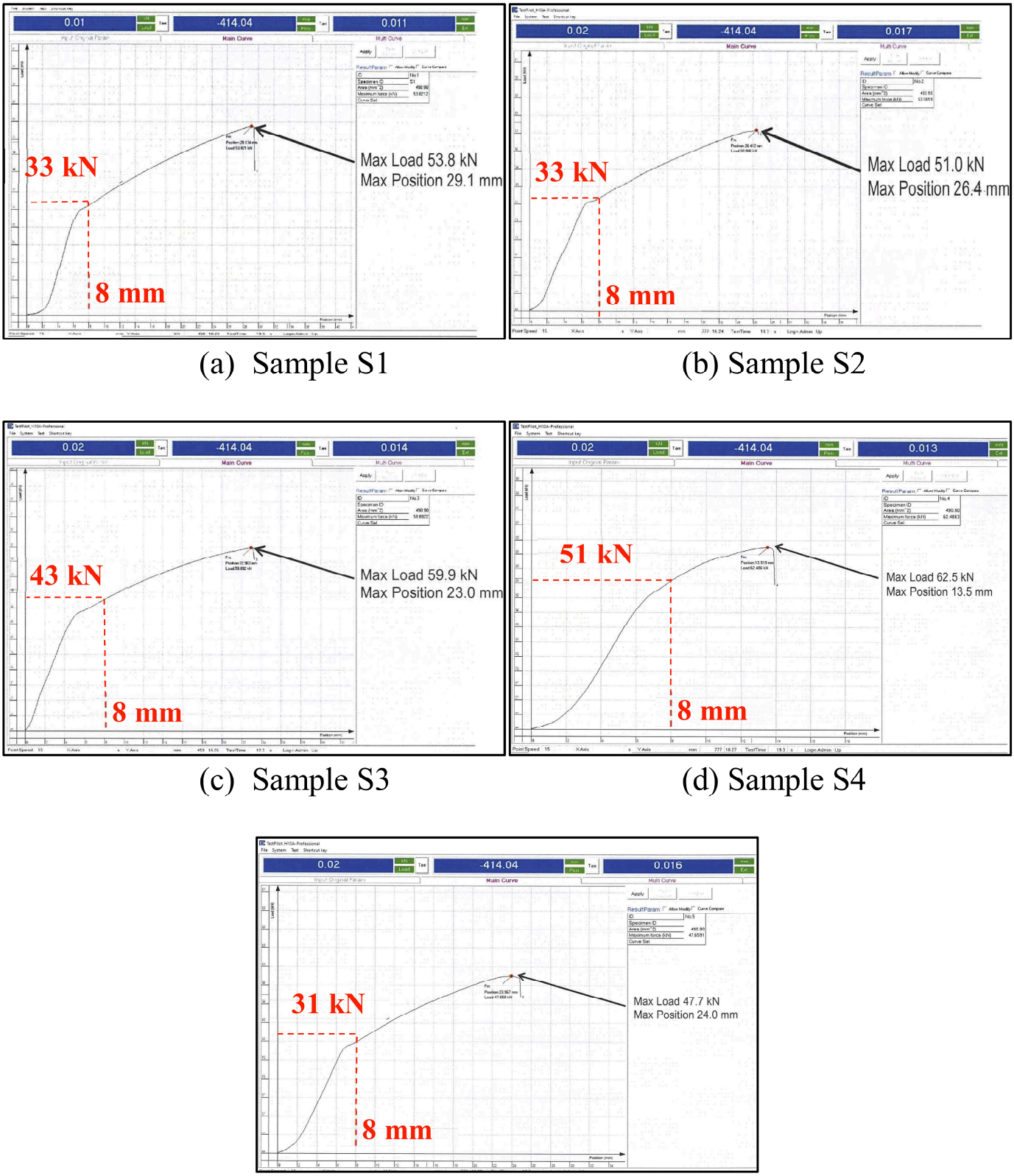

(a) Sample S1 (b) Sample S2

(c) Sample S3 (d) Sample S4

(e) Sample S5

Figure 12. Load vs. deformation curves under tensile testing for Samples S1~S5.

Table 7. Ultimate tensile force and corresponding deformation of sample tests.

Case	Test Sample	Ultimate Tension (kN)	Ultimate Deformation (mm)
Case 1	S1	53.8	29.1
	S2	51.0	26.4
	S5	47.7	24.0
Case 2	S3	59.9	23.0
Case 3	S4	62.5	13.5

4.2. Punching Shear Test

Three identical reinforced concrete wall panels (called as "W1"–"W3"), each with the dimension of 1000 mm × 1000 mm × 75 mm and incorporating H-shaped embeds as per Figure 13, were fabricated. The panels were designed based on a concrete strength with C45 and an assumed maximum aggregate size of 10 mm. The on-site slump measurement recorded 165 mm. Grade 500 MPa horizontal rebars T10-200 and vertical rebars T12-150 were used, with the embeds buried at a depth of 63 mm within the wall panels. Destructive punching shear tests were conducted on three panels. Additionally, compressive tests were performed on eight 100 mm × 100 mm × 100 mm cubes at 28-day age, resulting in an average compressive strength of 60.8 MPa.

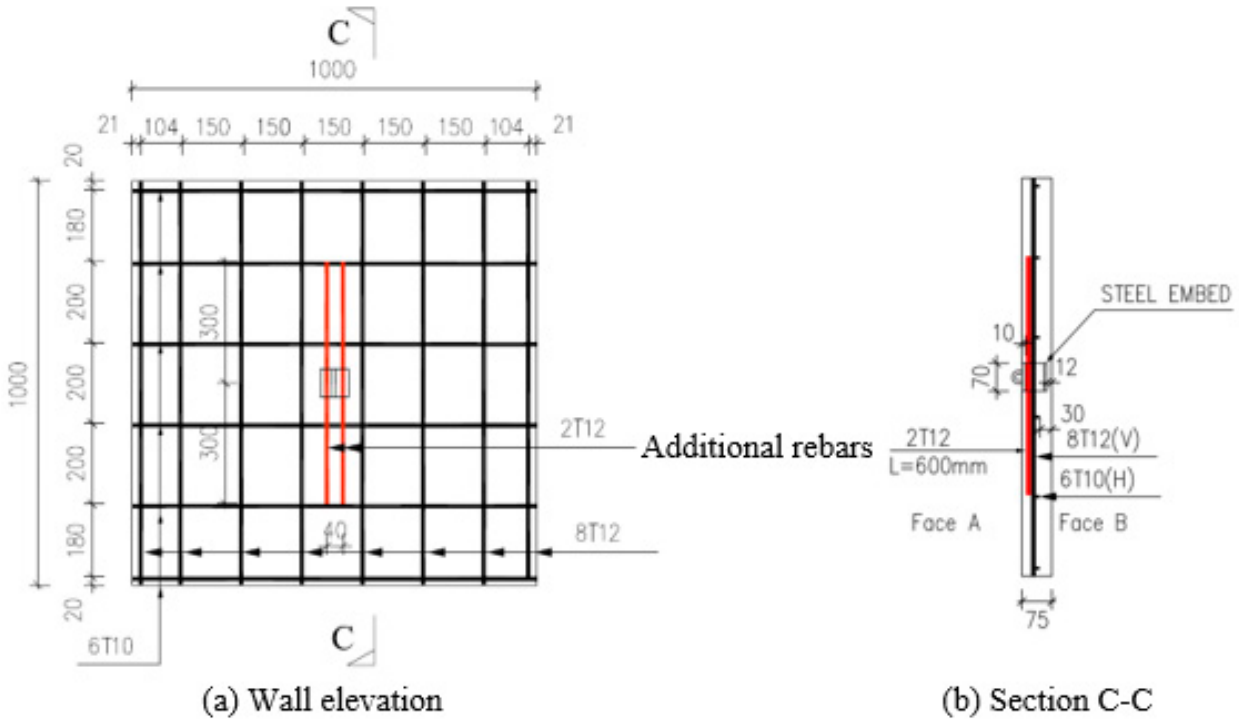

Figure 13. Wall panel details.

The loading reaction frame was fabricated using steel channels. The contact surface between the reaction frame and the wall panel had inner dimensions of 60 cm and outer dimensions of 80 cm. Loading was manually applied using hydraulic jacks and the pressure was measured through a pressure sensor. Figure 14 illustrates the test photos of wall panel W1. All three wall panels displayed brittle punching shear failure characteristics. Table 8 provides a summary of the test results for the three wall panels and estimates the average design punching shear capacity to be 35.6 kN, which was converted to be equivalent to grade C45 concrete.



Figure 14. Punching shear test for wall panel W1.

Table 8. Summary of three wall panels' punching shear test results.

Wall Panel Sample	Ultimate Punching Shear T_u (kN)	Design Punching Shear Capacity Equivalent to C45 Concrete T_{C45} (kN)	Average Capacity of T_{C45} (kN)
W1	47.1	34.1	
W2	56.3	40.7	35.6
W3	44.1	31.9	

Note: $T_{C45} = T_u \times (45/60.8)^{(1/3)}/1.25$, in which 1.25 is the partial safety factor for material strength.

5. Estimated Deformation and Further Analysis Modified by the Test Results

The test results were considered in FEA analysis (Figure 15a) for design checking of the side wall and inner tie. The stiffnesses of both the side wall and inner tie were taken into account. For the project example, in the project the inner tie system may be used, the model dimensions are as follows: height of 2.925 m, width of 2.775 m, and concrete design strength of C45. The side wall of the prefabricated module was simplified into a 1000 × 75 beam, the top slab into a 1000 × 100 beam, and the bottom slab into a 1000 × 115 beam. Additionally, two horizontal springs with a vertical spacing of about 1.0 m were added to each side wall to simulate the inner ties, maintaining horizontal spacing of no more than 1.0 m. The inner tie spring stiffness coefficient K can be determined using Equation (3) below.

$$K\ (kN/m) = T_{Test}/(0.008/2) \quad (3)$$

where T_{Test} represents the tension force of the inner tie at 8 mm deformation (referring to Table 5).

The range of spring stiffness coefficients falls between lower bound 7750 kN/m and upper bound 12,750 kN/m based on the test results of samples S1–S5. The input (spring stiffness coefficient) and output (horizontal displacement of side wall and unfactored inner tie tensile force) of further FEA analysis are summarized in Table 9. The analysis revealed that, under the influence of the concrete lateral pressure and with the spring stiffness coefficient at its lower bound value, the maximum elastic horizontal deformation of the side wall measures 3.5 mm as shown in Figure 15b, less than the allowable limit of 4 mm (equivalent to a total of 8 mm horizontal deformation on both side walls). Moreover, with the spring stiffness coefficient set to its upper bound value, the maximum unfactored tensile force of the inner tie reached 27.2 kN. When multiplied by the minimum load safety factor

of 1.2 under the construction condition [20], the design tensile force is computed at 32.6 kN, which remains below both the C45 concrete wall panel's average design punching shear resistance of 35.6 kN and Sample S4's design tensile resistance of 56.8 kN (calculated as 62.5 kN/1.1).

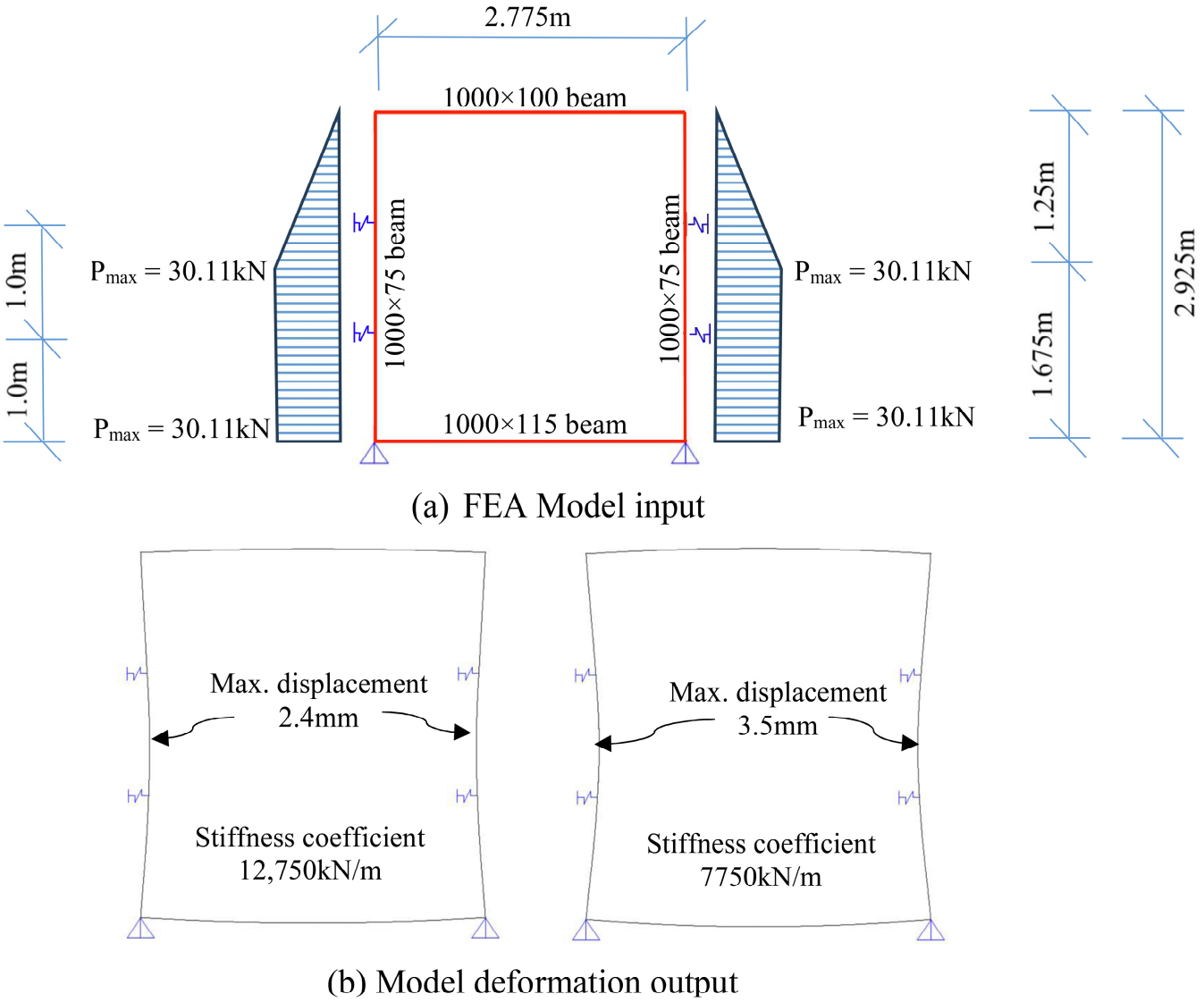

Figure 15. FEA model input and output.

Table 9. Summary of major input and output in FEA frame model.

		FEA Input	FEA Output	
Test Sample	**Tension at 8 mm Deformation T_{Test} (kN)**	**Inner Tie Stiffness (kN/m)**	**Hor. Displacement of Side Wall (mm)**	**Unfactored Inner Tie Tensile Force (kN)**
S4	51	12,750 (Upper bound)	2.4 (<4.0, OK)	27.2 (27.2 × 1.2 * = 32.6 < 35.6, OK)
S5	31	7750 (Lower bound)	3.5 (<4.0, OK)	23.6 (23.6 × 1.2 * = 28.3 < 35.6, OK)

Note: * The minimum load safety factor is 1.2 under the construction condition [20].

6. Practical Application

6.1. Application Scope of the Inner Tie System

The inner tie system can be used in a MiC composite wall with the design total thickness between 250 mm and 500 mm as shown in Figure 16. This thickness range can cover most MiC composite wall cases, where the side wall cannot resist deformation by itself within a certain limit under wet concrete pouring load. If the total wall thickness is less than 250 mm, the gap between precast walls will be too narrow to place the inner tie in. And a total wall thickness larger than 500 mm is seldom needed in a MiC project.

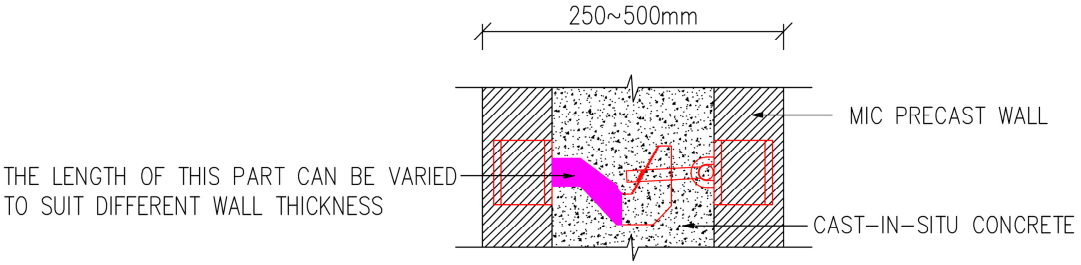

Figure 16. Design thickness of a composite wall.

6.2. Mockup Assembly and Monitoring

Four 1:1 MiC mockup modules (by two in each floor as shown in Figure 17) were prefabricated for trial assembly, and then concrete was cast in one go into the gap between modules. During concrete pouring, the horizontal deformation of the side walls of the modules was measured through displacement sensors which sit on the module's bottom slab (as shown in Figures 18 and 19). The measured deformation of the side wall after concrete pouring on-site does not exceed 3.2 mm (Figure 20), which is consistent with the estimated analysis results in Section 5.

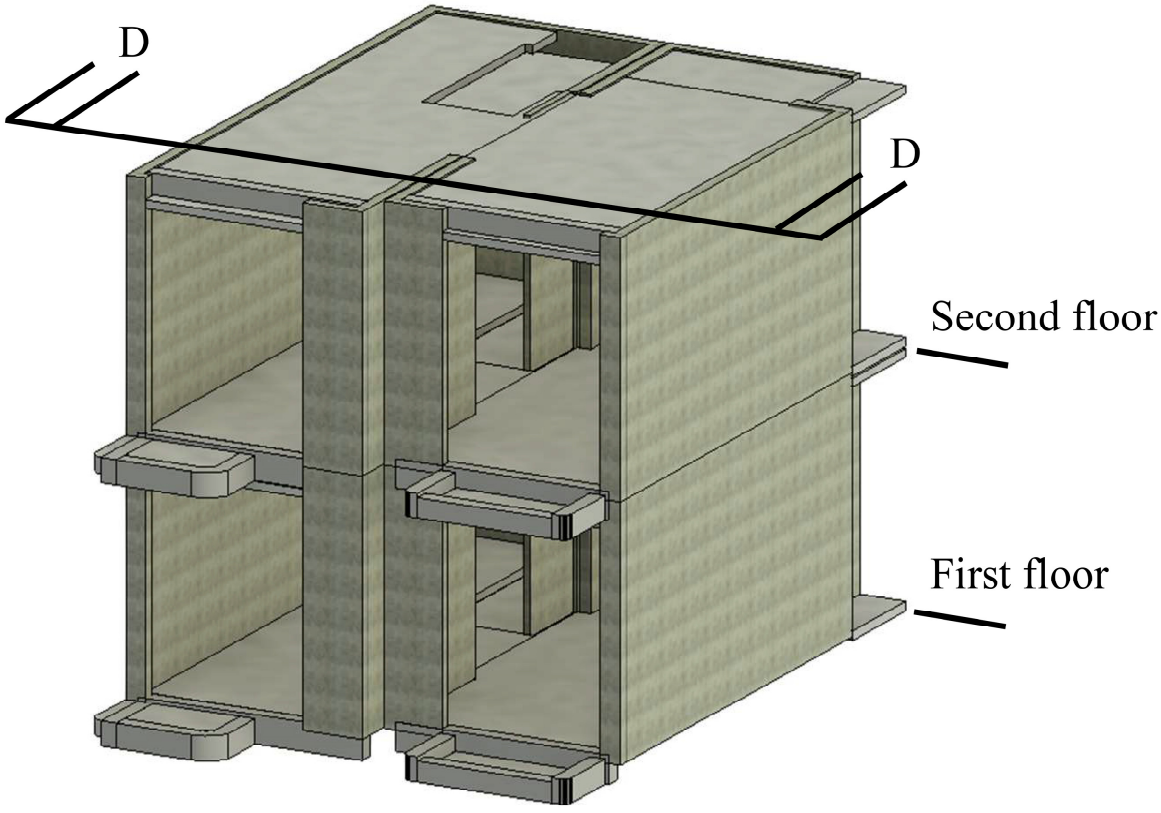

Figure 17. The 3D BIM view for four mockup modules.

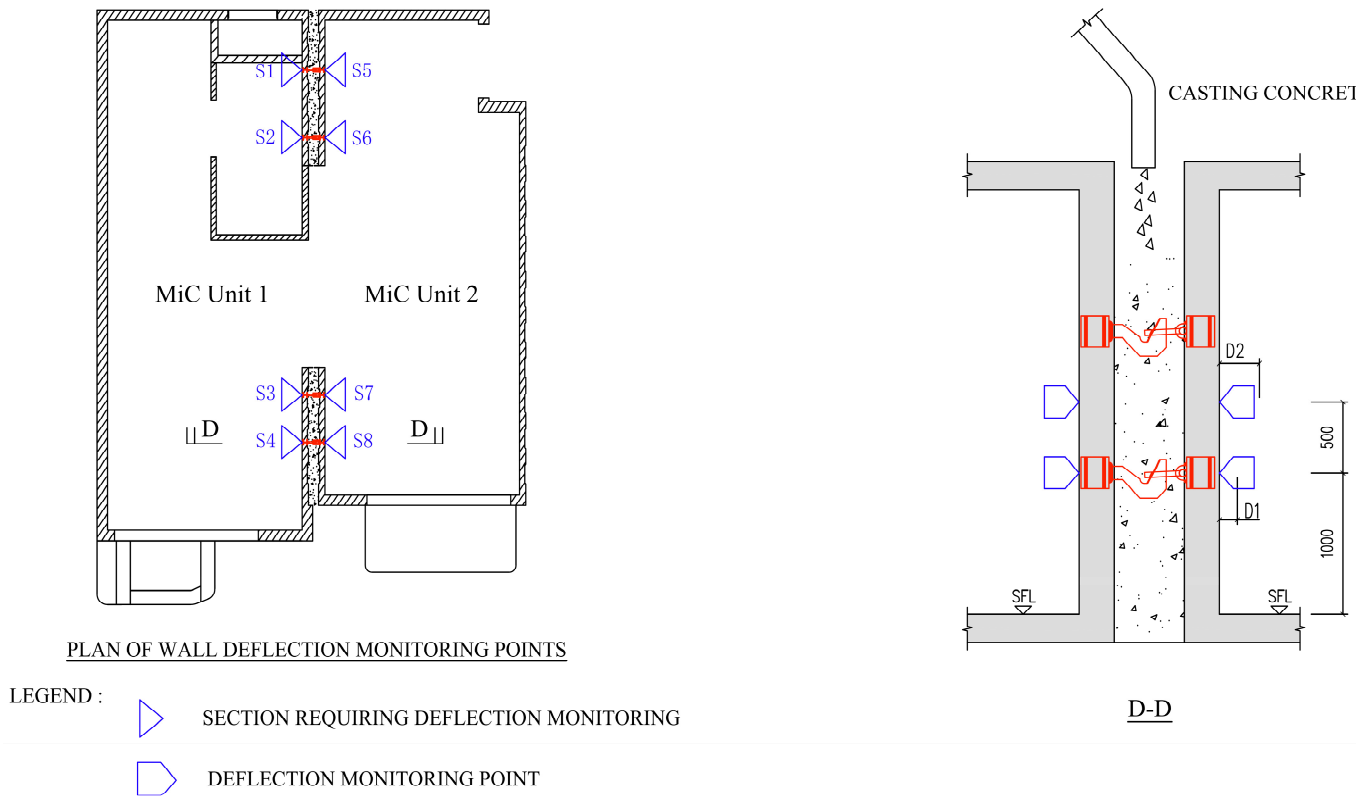

Figure 18. Deflection monitoring points for a MiC module side wall.

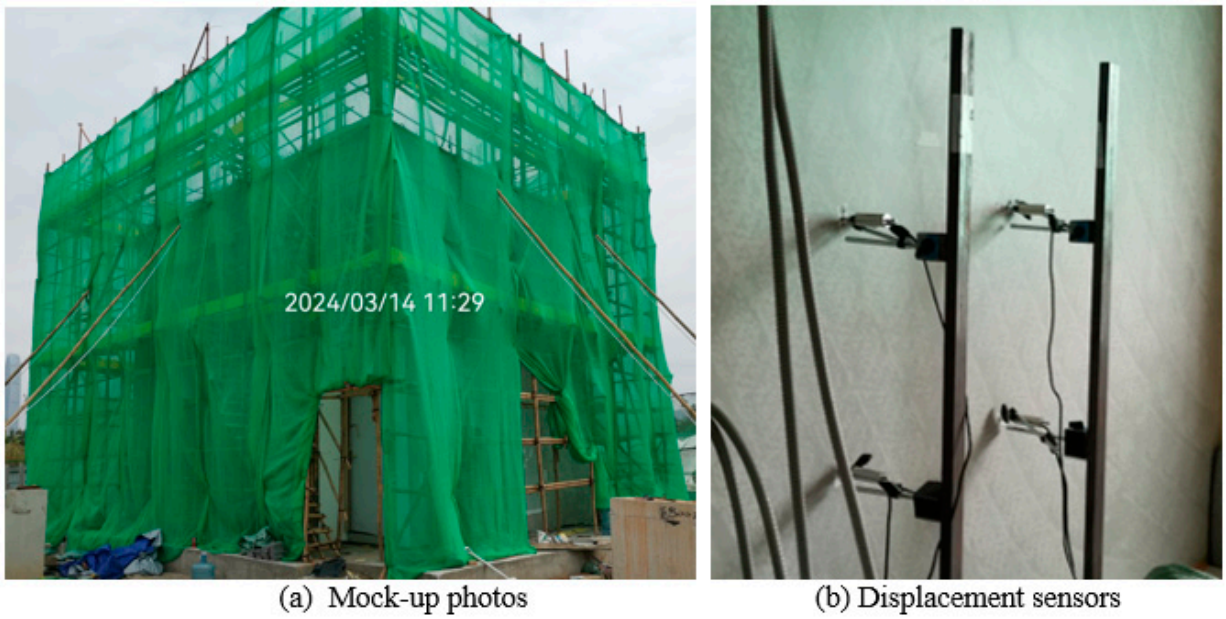

Figure 19. Photos for instrumented mock-up assembly.

6.3. Application in a Real Project

Based on analysis and testing, the inner tie systems were integrated into a four-storey reinforced concrete MiC project in Hong Kong (as shown in Figure 21). The full set design submission was approved by local authoritative departments. The project involved 106 MiC modules (i.e., 90 composite walls) with a total of 1048 sets of inner ties. As the side walls

deformation can be well controlled by inner ties, the on-site concrete pouring of each composite wall with the inner ties were carried out.

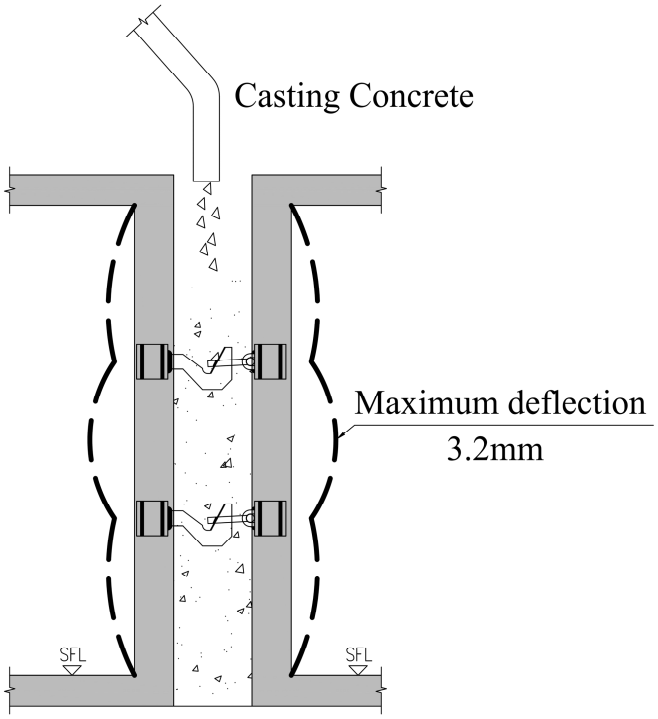

Figure 20. Side wall deformation curve and maximum deformation.

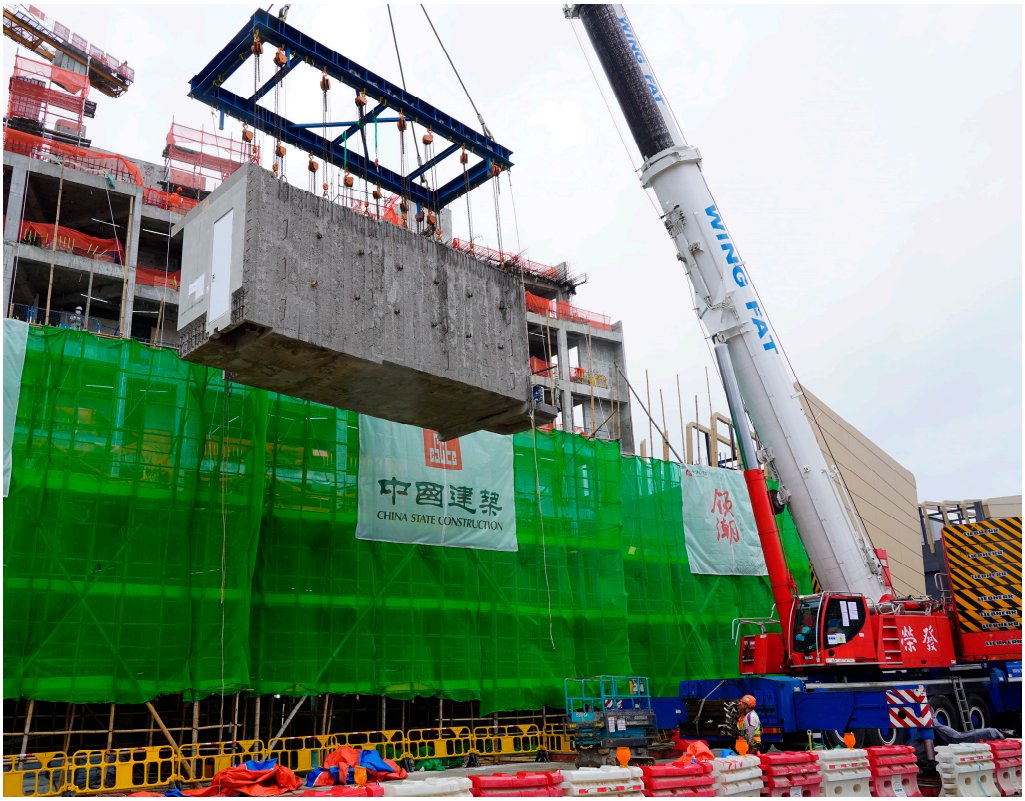

Figure 21. Erection of MiC module.

Compared to the traditional tying method of through-bolts penetrating precast side walls, inner ties saved about one month construction time and several million HKD con-

struction cost for this project. The application of inner ties avoided the need to repair the precast side walls and carry out interior decorations on site.

The most challenging aspect of the project was in controlling the construction errors of the embeds, hooks, and loops to be within allowed fabrication tolerance ±3mm in the prefabrication factory. Their positioning dimensions were checked and recorded before precasting MiC modules and welding hooks and loops to embeds, respectively. As for the on-site installation of MiC modules, it is also very important to control the construction error so as not to exceed the allowed installation tolerance of ±5 mm. Otherwise, the module position shall be finely adjusted.

7. Conclusions

To address the challenge of securing prefabricated side walls during the concrete casting process for a composite wall in a reinforced concrete MiC project, a new inner tie system was invented and presented in this paper. This system does not need to penetrate through MiC module side walls and allows for full decoration of the MiC module in the factory while reducing on-site workload. It is not only easy to install and reliable to take the load, but also adaptable to a certain construction error and capable of reducing the thickness and weight of the prefabricated side walls. This system offers both temporary tying for the prefabricated side walls during the casting process and permanent tying in the composite wall. A series of technical efforts were made by member size optimization using Ansys software V16, tensile testing of the steel component, punching shear testing of the reinforced concrete wall panel, further analysis incorporating testing results, and instrumented mockup assembly for the inner tie system. The system was finally successfully implemented in a real MiC project in Hong Kong. The time for on-site concrete casting of composite walls was saved and the horizontal deformations of MiC module side walls were well controlled within an allowable limit.

Next, the system can be further improved to enhance its robustness and broaden its potential application across various projects. The practical application will bring a valuable reference for other MiC projects.

Author Contributions: Data curation, Writing—review & editing, Methodology, X.Z.; Investigation, Methodology, J.H.; Writing—original draft, Software, W.L.; Investigation, Visualization, J.S.; Investigation, Visualization, S.A.; Investigation, Validation, Z.Z.; Data curation, Validation, T.S.; Formal analysis, D.K.; Formal analysis, Y.Z. All authors have read and agreed to the published version of the manuscript.

Funding: This research was funded by China State Construction Engineering (Hong Kong) Ltd.

Data Availability Statement: Data are contained within the article.

Acknowledgments: The R&D funding support for "Research on Key Connections of Reinforced Concrete Modular Integrated Construction Structures" from China State Construction Engineering (Hong Kong) Ltd. is gratefully acknowledged. We would like to express our sincere gratitude to Yaopeng Liu for providing FEA software Ansys analysis for this research. We would also like to extend our heartfelt thanks to Zhongcai He, Chenghua He, and Chimun Lo for site supervision during MiC construction in a Hong Kong project.

Conflicts of Interest: All authors were employed by the company China State Construction Engineering (Hong Kong) Ltd. The authors declare no conflict of interest. The authors declare that this study received funding from China State Construction Engineering (Hong Kong) Ltd. The funder was not involved in the study design, collection, analysis, interpretation of data, the writing of this article or the decision to submit it for publication.

References

1. Hu, H.S.; Xia, H.J. A Type of Modular Shear Wall Structure and Its Construction Method. China Patent CN115807499B, 25 April 2023.
2. Ji, J.; Huang, G.X.; Feng, Z.H.; Lin, J.C.; Chen, Q.J.; Tan, Z.X.; Li, P.L. A Type of Composite Modular Integrated Construction Structure. China Patent CN115045534A, 13 September 2022.

3. Duan, L.J.; Yu, Y.S.; Wang, T.; Fu, C.C. Experimental Research on Mechanical Behavior of Prefabricated Prefinished Volumetric Construction Connections. *J. Qingdao Univ. Technol.* **2022**, *43*, 1–7.
4. Pan, W.; Wang, Z.; Zhang, Y.; Zhang, Z.Q. Horizontal Connection Joint and Construction Method of Multi-Story and High-Rise Concrete MiC Buildings. China Patent CN116084591A, 9 May 2023.
5. Li, Z.; Wang, Q.; Zhang, J.Y.; Chen, C.J.; Zhang, Z.; Ding, T.; Chen, J.; Lan, Z.L.; Zhang, Y. A Type of MiC Building with Mixed Wall Structures. China Patent CN219794297U, 3 October 2023.
6. Yao, J.; Huang, M.Y.; Zeng, Z.X.; Wu, C.; Zeng, W.L.; Xu, X.; Tan, P.; Ding, T. A Type of Concrete MiC Module. China Patent CN219527957U, 15 August 2023.
7. Poon, C.M.; Ma, M.C.; Li, Z.; Zhang, Z.; Chen, Z.H.; Xie, J.H.; Mei, K.L.; Liu, Y.L. A Type of Concrete MiC Structural System and Its Construction Method. China Patent CN117127714A, 28 November 2023.
8. Qaidi, S.M.A.; Tayeh, B.A.; Zeyad, A.M.; de Azevedo, A.R.G.; Ahmed, H.U.; Emad, W. Recycling of mine tailings for the geopolymers production: A systematic review. *Case Stud. Constr. Mater.* **2022**, *16*, e00933. [CrossRef]
9. Qaidi, S.M.A.; Dinkha, Y.Z.; Haido, J.H.; Ali, M.H.; Tayeh, B.A. Engineering properties of sustainable green concrete incorporating eco-friendly aggregate of crumb rubber: A review. *J. Clean. Prod.* **2021**, *324*, 129251. [CrossRef]
10. Izadifar, M.; Dolado, J.S.; Thissen, P.; Ukrainczyk, N.; Koenders, E.; Ayuela, A. Theoretical Elastic Constants of Tobermorite Enhanced with Reduced Graphene Oxide through Hydroxyl vs. Epoxy Functionalization: A First-Principles Study. *J. Phys. Chem. C* **2023**, *127*, 18117–18126. [CrossRef]
11. Zou, X.K.; Huang, J.; Lu, W.J.; Shi, J.; Zhao, Z.; Shi, T. A New Composite Wall Inner Tie System Applied in Reinforced Concrete Modular Integrated Construction. In Proceedings of the 10th International Conference on Construction Engineering and Project Management, Sapporo, Japan, 29 July–1 August 2024; pp. 85–92.
12. Chan, C.M.; Zou, X.K. Elastic and Inelastic Drift Performance Optimization for Reinforced Concrete Buildings under Earthquake Loads. *Earthq. Eng. Struct. Dyn.* **2004**, *33*, 929–950. [CrossRef]
13. Zou, X.K.; Chan, C.M. Optimal Seismic Performance-Based Design of Reinforced Concrete Buildings Using Nonlinear Pushover Analysis. *Eng. Struct.* **2005**, *27*, 1289–1302. [CrossRef]
14. Zou, X.K.; Chan, C.M. An Optimal Resizing Technique for Seismic Drift Design of Concrete Buildings Subjected to Response Spectrum and Time History Loadings. *Comput. Struct.* **2005**, *83*, 1689–1704. [CrossRef]
15. Zou, X.K.; Chan, C.M.; Li, G.; Wang, Q. Multiobjective Optimization for Performance-Based Design of Concrete Structures. *J. Struct. Eng.* **2007**, *133*, 1462–1474. [CrossRef]
16. Zou, X.K.; Teng, J.G.; Xia, S.H.; Wong, Y.L. Optimal Performance-Based Seismic Retrofit Design of FRP-confined Concrete Buildings. *Compos. Part B Eng.* **2007**, *38*, 584–597. [CrossRef]
17. Zou, X.K.; Wang, Q.; Li, G.; Chan, C.M. Integrated Reliability-Based Seismic Drift Design Optimization of Base-Isolated Concrete Buildings. *J. Struct. Eng.* **2010**, *136*, 1282–1295. [CrossRef]
18. Zou, X.K.; Zhang, Y.; Liu, Y.P.; Shi, L.C.; Kan, D. Design and Construction of High-Performance Long-Span Steel Transfer Twin Trusses Applied in One Hospital Building in Hong Kong. *Buildings* **2023**, *13*, 751. [CrossRef]
19. Clear, C.A.; Harrison, T.A. *CIRIA Report 108—Concrete Pressure on Formwork*; Construction Industry Research and Information Association: London, UK, 1985.
20. Buildings Department of Hong Kong SAR Government. *Code of Practice for the Structural Use of Steel 2011*, 2023 ed.; Buildings Department of Hong Kong SAR Government: Hong Kong, China, 2023.

Disclaimer/Publisher's Note: The statements, opinions and data contained in all publications are solely those of the individual author(s) and contributor(s) and not of MDPI and/or the editor(s). MDPI and/or the editor(s) disclaim responsibility for any injury to people or property resulting from any ideas, methods, instructions or products referred to in the content.